Eur. Phys. J. B **26**, 41–50 (2002)
DOI: 10.1140/epjb/e20020064

THE EUROPEAN PHYSICAL JOURNAL B
EDP Sciences

Solid-state reaction in Ti/Ni multilayers studied by magneto-optical and optical spectroscopies, and X-ray diffraction

Y.P. Lee[1,a], K.W. Kim[2], Y.V. Kudryavtsev[3], V.V. Nemoshkalenko[3], and B. Szymański[4]

[1] Department of Physics, Hanyang University, 17 Haengdang-Dong, Sungdong-Ku, Seoul, 133-791, Korea
[2] Department of Physics, Sunmoon University, 100 Galsan-Ri, Tangjeong-Myeon, Asan, Choongnam, 336-840, Korea
[3] Institute of Metal Physics, National Academy of Sciences of Ukraine, 36 Vernadsky str., Kiev-142, Ukraine
[4] Institute of Molecular Physics, Polish Academy of Sciences, 17 Smoluchowskiego str., 60-179 Poznań, Poland

Received 2 May 2001 and Received in final form 21 November 2001

Abstract. Comparative study of the solid-state reaction (SSR) in a series of Ti/Ni multilayered films (MLF) with a bilayer period of 0.65–22.2 nm and a constant Ti to Ni sublayer thickness ratio has been performed by using the experimental and computer-simulated magneto-optical (MO) and optical spectroscopies as well as X-ray diffraction (XRD). It was shown that alloyed-like regions in an amorphous structure is spontaneously formed near the interfaces between pure elements during the film deposition. The thickness of this region was estimated as 2–3.8 nm on the basis of the MO and optical studies. The SSR in the Ti/Ni MLF caused by an annealing at 580 K for 60 min increases the thickness of these interfacial amorphous regions. It was shown that SSR takes place mainly in the Ti/Ni MLF with relatively "thick" sublayers. The existence of a threshold nominal Ni-sublayer thickness for observing the equatorial Kerr effect of about 3.0 and 4.5 nm for the as-deposited and annealed Ti/Ni MLF, respectively, is explained by formation of the nonmagnetic alloyed regions between pure components during the film deposition as a result of the SSR. For the case of Ti/Ni MLF, the MO and optical approaches turn out to be more sensitive in determining the thickness of the reacted zone, while XRD is more useful for the structural analysis. It was also shown that the very thin nonreacted Ni sublayers have different MO properties (and hence electronic structure) from the bulk.

PACS. 68.35.Fx Diffusion; interface formation – 68.65-k Low-dimensional, mesoscopic, and nanoscale systems: structure and nonelectronic properties – 71.55.Jv Disordered structures; amorphous and glassy solids – 75.70.-i Magnetic properties of thin films, surfaces, and interfaces

1 Introduction

Ti/Ni multilayered films (MLF) can be considered as an ideal candidate for neutron optics, in particular, in neutron guides and focusing devices, because they have an excellent contrast factor for thermal and cold neutrons. In addition, Ni and Ti are magnetic and nonmagnetic materials, respectively, and therefore, the Ti/Ni MLF can be used for polarizing neutrons [1,2]. The neutron reflectivity of the Ti/Ni MLF is strongly influenced by their interfacial properties [3]. To understand the properties of the MLF, it is important to know how sharp the interfaces between sublayers are.

On the other hand, this system is also interesting owing to the tendency of amorphization through a solid-state reaction (SSR) [4]. The Ti-Ni system satisfies the main conditions for the occurrence of the SSR. These conditions are: a large and negative heat of mixing, an anomalous diffusion of Ni in Ti, and a low mobility for one of the elements in the amorphous phase [5]. The difference in mobility of the Ti and Ni atoms plays a kinetic constraint for the stability of amorphous phase at comparatively low temperatures. Therefore, the Ti/Ni MLF can be also considered as a model object for the investigation of the SSR.

A lot of experimental techniques are usually involved for the study of the SSR in multilayered systems: differential scanning calorimetry [5,6], Auger electron spectroscopy [7], X-ray photoelectron spectroscopy [8,9], various magnetic methods [10], and, of course, the traditional direct methods, *i.e.*, X-ray diffractometry and transmission electron microscopy [11]. Each method has its own specific features and has advantages and disadvantages for this study. Therefore, a more complete information on the SSR can be obtained by employing the several experimental techniques.

[a] e-mail: yplee@hanyang.ac.kr

Table 1. Parameters of the investigated Ti/Ni MLF. N is the number of repetition, $h_{\mathrm{Ti(Ni)}}$ is the nominal thickness of the Ti(Ni) sublayers, $t_{\mathrm{Ti(Ni)}}$ is the measured thicknesses of Ti(Ni) sublayers, T is the total thickness of the MLF.

Sample No.	N	h_{Ti} (nm)	h_{Ni} (nm)	t_{Ti} (nm)	t_{Ni} (nm)	T (nm)	Ni content (at.%)
1	15	10.0	10.0	10.4	11.8	333.0	64.6
2	20	7.5	7.5	8.0	8.8	336.0	64.0
3	30	5.0	5.0	5.2	6.0	336.0	65.0
4	43	3.5	3.5	3.9	4.2	348.3	63.5
5	60	2.5	2.5	3.2	3.0	372.0	60.2
6	600	0.25	0.25	0.31	0.34	390.0	63.9
7	alloy					300.0	62.5

It is well known that both magneto-optical (MO) and optical properties of metals depend strongly on their electron energy structures which are correlated with the atomic and magnetic ordering. The interdiffusion between Ti and Ni atoms in the Ti/Ni MLF caused by a low temperature annealing should decrease the thickness of pure Ni (and hence the magnetic and MO response) as well as the change in chemical and atomic ordering in the reactive zone. In contrast to the usual magnetic methods or the single-wave MO loop tracing, it can be expected that the application of MO spectroscopy to the study of the SSR in the Ti/Ni MLF allows us to obtain additional information on the changes in atomic and chemical ordering in the reactive zone. On the contrary to MO spectroscopy, optical spectroscopy has no restriction on the magnetic state of the constituent sublayers. Evidently, the real structures and magnetic properties of the as-deposited and reacted MLF may be verified by a comparison between experimental and computer-simulated MO and optical data, based on an appropriate model for the structure of the MLF and the properties of the constituent sublayers. To the best of our knowledge, the MO and optical spectroscopy have not been used for this purpose. At the same time, the MO and optical properties themselves of the Ti/Ni MLF have not been investigated yet.

In this work we applied a new method for studying the SSR in the Ti/Ni MLF, which is based on the comparison between spectroscopic computer-simulated and experimental MO and optical properties of the as-deposited and annealed multilayers, with also referring to the results of structural analysis by the traditional X-ray diffraction (XRD). The comparison with the published results based on other methods was also carried out [5,11].

2 Experimental and simulation details

A series of Ti/Ni MLF with a bilayer period of 0.65–22.2 nm and a nearly constant (1:1) sublayer thickness ratio, and a total thickness of about 330 nm were prepared by using the computer-controlled double-pair target face-to-face sputtering onto glass substrates at room temperature (RT). Table 1 contains the parameters for the prepared and investigated Ti/Ni MLF. All the Ti/Ni MLF have a Ti sublayer at the top. The sublayer thicknesses in the MLF were estimated by X-ray fluorescence. The X-ray fluorescence data were additionally confirmed by low-angle X-ray diffraction. The structures of samples were analyzed by using low- and high-angle XRD.

The details of the experimental study of the MO and optical properties of the Ti/Ni MLF can be found elsewhere [12]. After the measurement of MO and optical properties of the as-deposited samples, a SSR in the Ti/Ni MLF was induced by an annealing at 580 K for 60 min in a high vacuum and then their structures, MO and optical properties were studied again.

It is known that, for the simulation of the MO and optical properties of MLF, the MO and optical properties of the constituent sublayers should be known in advance. In order to use in the simulation the MO and optical parameters of the constituent sublayers relevant to the prepared Ti/Ni MLF, pure Ti and Ni as well as $Ti_{0.38}Ni_{0.62}$ alloy films of about 100 nm in thickness were also prepared at the same deposition conditions, and their MO and optical properties were also investigated. The composition of $Ti_{0.38}Ni_{0.62}$ alloy nearly corresponds to the overall compositions of the Ti/Ni MLF (see Tab. 1).

The theoretical simulations of the equatorial Kerr effect (EKE) spectra and optical properties for the Ti/Ni MLF were performed by solving exactly a multireflection problem using the scattering matrix approach [13], assuming several models of the MLF. These models are: a) MLF with "sharp" (ideal) interfaces resulting in rectangular depth profiles of pure Ti and Ni; b) MLF with "mixed" (alloy-like) interfaces of variable thickness between pure-metal sublayers; and c) MLF with sharp interface and partly "dead" (in magnetic sense) Ni sublayers. It is clear that the composition in the actual mixed interfacial region is gradually changed from, for example, pure Ti through Ti-Ni alloy to pure Ni. Nevertheless, for the simplicity in the calculations, the actual interfacial structure was represented by an idealized case of $Ti_{0.38}Ni_{0.62}$ alloy between pure Ni and Ti sublayers. We also supposed that the consumption of pure Ti and Ni for formation of Ti-Ni alloy is carried out in a symmetrical way to form $Ti_{0.38}Ni_{0.62}$ alloy. For the nonmagnetic (or magnetically "dead") Ni layers, the off-diagonal components of the dielectric function (DF) were equalized to zero.

3 Results and discussion

3.1 X-ray diffraction study

Low-angle XRD patterns for the as-deposited Ti/Ni MLF confirmed their layered structure down to the nominal sublayer thickness of about 3 nm (sample No. 5) (see Fig. 1). The raw high-angle XRD patterns for the as-deposited Ti/Ni MLF, together with pure Ni and $Ti_{0.38}Ni_{0.62}$ alloy films, are shown in Figure 2a. It is seen that only the Ni (111) sharp diffraction peak is observed at $2\Theta_{\max} = 44.62°$ for the pure Ni film. The Ni lattice spacing calculated from the Ni (111) peak position reveals $d_{\mathrm{Ni(111)}} = 0.2029$ nm which is very close to the literature

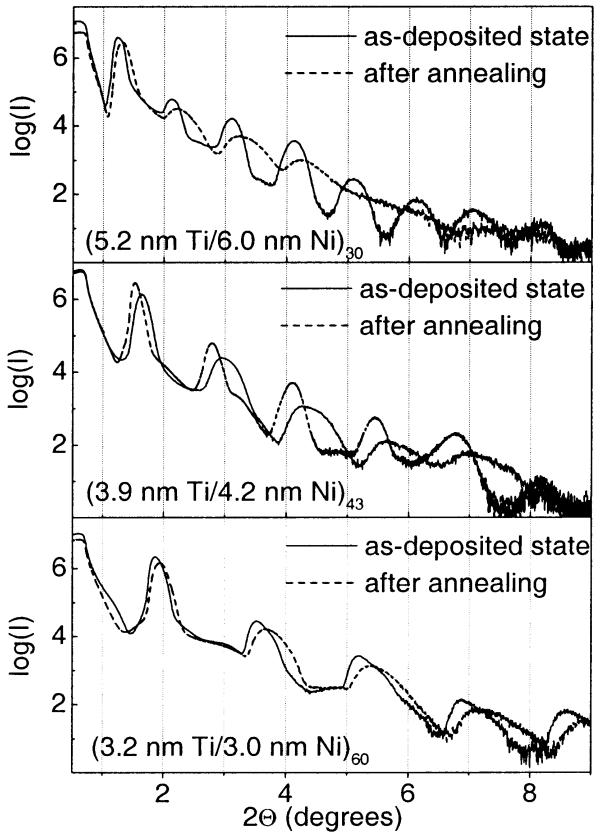

Fig. 1. Low-angle X-ray diffraction patterns for the as-deposited and annealed Ti/Ni MLF (sample Nos. 3–5).

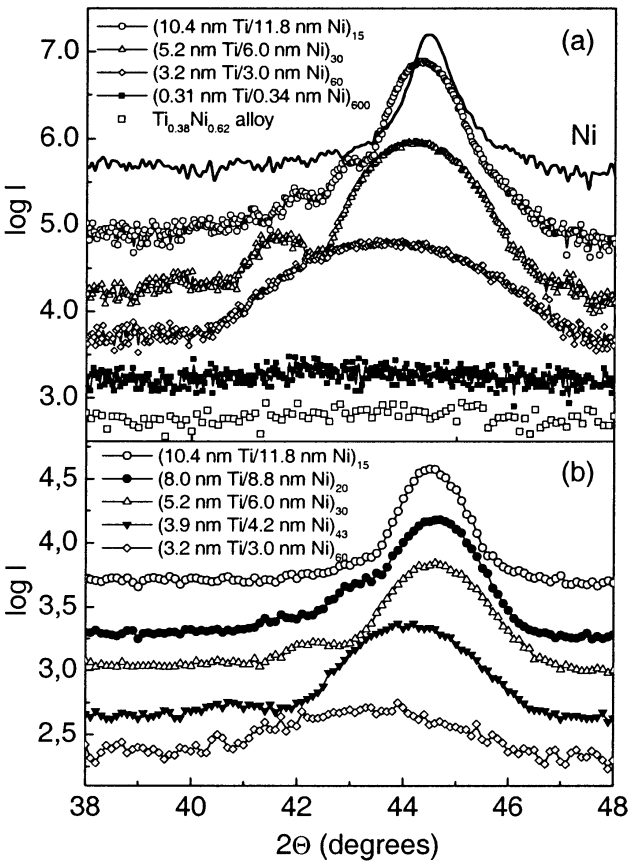

Fig. 2. X-ray diffraction patterns for the (a) as-deposited and (b) annealed Ti/Ni MLF, as well as for $Ti_{0.38}Ni_{0.62}$ alloy and pure Ni films. For the convenience of presentation all the curves are shifted upward relatively lowest plot.

data for bulk Ni ($d_{\mathrm{Ni}(111)} = 0.2034$ nm) [14]. On the contrary to the Ni diffraction peak, any visible manifestation of Ti is not observed in the XRD spectra for the investigated Ti/Ni MLF. Such a behavior can be explained by the formation at our deposition conditions of textureless fine grains or an amorphous structure in the Ti sublayers, because even the XRD pattern for the prepared pure Ti film exhibits only a weak and broad peak located at $2\Theta_{\max} = 36.62°$ which is attributed to the Ti (002) reflection.

The detailed analysis of the obtained results for the as-deposited (and annealed) Ti/Ni MLF have been performed. For this purpose the background for each high-angle XRD spectrum was subtracted, first of all, and then a multiple-peak fitting procedure was employed for the remanent spectrum. Figure 3 illustrates this process in detail for sample No. 3 as an example.

Such a deconvolution allowed us to determine the exact angular positions $2\Theta_{\max}$, height (I_{h}) and integrated (I_{i}) intensities, and full width at half maximum (FWHM) ξ for all the constituent peaks. The results related to the most-intense constituent peak are tabulated in Table 2.

It is known that the integral breadth of the diffraction peak $\beta(\equiv I_{\mathrm{i}}/I_{\mathrm{h}})$ is inversely proportional to the size Z of the coherently diffracting domains in the direction perpendicular to the diffraction planes [11]. On the other hand, if the peak shape remains constant during the annealing, the change in ξ is also inversely proportional to

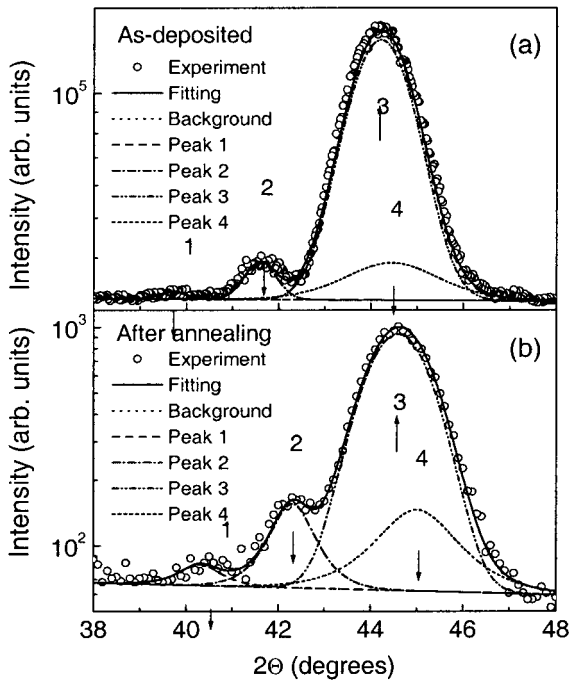

Fig. 3. Multiple peak analyses of X-ray diffraction patterns for the (a) as-deposited and (b) annealed Ti/Ni MLF (sample No. 3).

Table 2. Parameters of the main diffraction peak for as-deposited and annealed Ti/Ni MLF. State 1 and 2 indicate the as-deposited and annealed states, respectively.

State of the MLF	Sample No.	t_{Ni} (nm)	$2\Theta_{max}$ (°)	ξ (°)	β
1	Ni	100.0	44.62	0.54	0.178
1	1	11.8	44.35	0.93	0.077
1	3	6.0	44.21	1.60	0.130
1	5	3.0	43.70	3.10	2.189
1	6	0.34	44.04	6.04	-
1	7	-	44.32	5.50	-
2	1	11.8	44.54	1.10	0.367
2	2	8.8	44.59	1.50	0.498
2	3	6.0	44.59	1.62	0.536
2	4	4.2	44.12	2.12	0.681
2	5	3.0	43.38	3.30	0.595

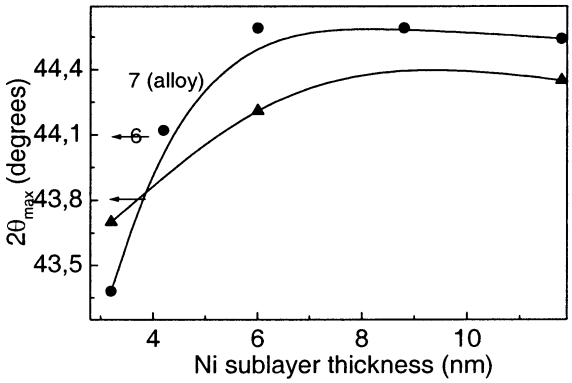

Fig. 4. Change in $2\Theta_{max}$ with t_{Ni} dependence for the as-deposited (triangles) and annealed (circles) Ti/Ni MLF. Arrows with numbers 6 and 7 indicate $2\Theta_{max}$ for samples 6 and 7 ($Ti_{0.38}Ni_{0.62}$ alloy film).

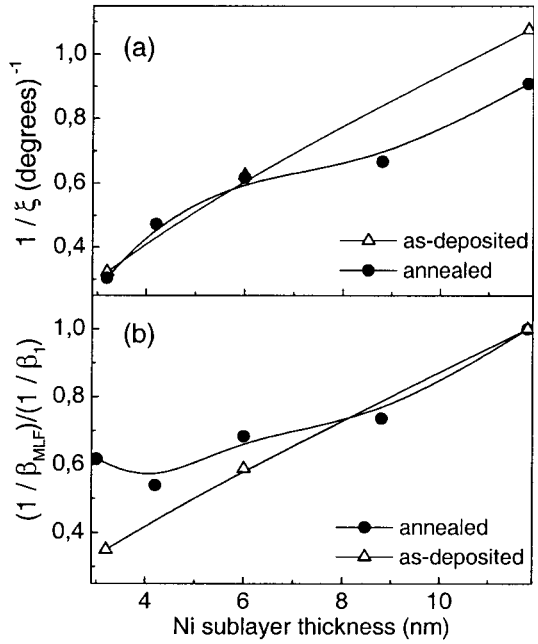

Fig. 5. Ni sublayer thickness dependences of the (a) reciprocal FWHM of the Ni (111) diffraction peak and (b) normalized $1/\beta$ with respect to sample 1 for the as-deposited (triangles) and annealed (circles) Ti/Ni alloy films.

Z and the mean grain size. A part of the obtained results relevant to the main diffraction peak is presented in Table 2 and shown as a function of the Ni sublayer thickness in Figures 4 and 5. It should be noticed here that the lines in Figure 4 are only the guide for eye.

In comparison with the pure Ni film, the main (Ni (111)) diffraction peak for the as-deposited Ti/Ni MLF with a "thick" Ni sublayer (sample Nos. 1–3) is slightly smeared and shifted to the low-angle side, and the smearing and shift increases with decreasing the sublayer thickness (see Figs. 2a, 4 and Tab. 2). The (0.31 nm Ti / 0.34 nm Ni)$_{600}$ MLF has an high-angle XRD spectrum similar to that for the $Ti_{0.38}Ni_{0.62}$ alloy film which was prepared by co-sputtering of the Ti and Ni targets. Both XRD spectra are significantly different from the others: they exhibit a very tiny and broad diffraction peak at $2\Theta_{max} \approx 44.0$–$44.3°$, manifesting the formation of a highly disordered or amorphous structure (see Fig. 2a). It should be mentioned here that, besides the main peak and a weak low-angle satellite peak, a fitting procedure also revealed for Ti/Ni MLF with a "thick" sublayers a broad peak nearly at the same angles, *i.e.*, at 44.45°, whose existence was not obvious from the visual inspection of the raw data (see, for example, peak 4 in Fig. 3). The as-deposited (3.2 nm Ti / 3.0 nm Ni)$_{60}$ MLF shows an XRD spectrum whose shape belongs to an intermediate between both groups of samples, exhibiting a broad diffraction maximum at $2\Theta_{max} \approx 43.7°$. The observed peak can be related to a strongly smeared Ni (111) peak but more probably to a significantly broadened peak originating from the monoclinic NiTi (002) or Ni_3Ti (004) diffraction peaks ($2\Theta_{NiTi(002)} \approx 43.914°$ and $2\Theta_{Ni_3Ti(004)} \approx 43.691°$).

In contrast to the pure Ni film, the XRD spectra of the Ti/Ni MLF with "thick" sublayers also reveal the Laue satellites on the low-angle side of the Ni (111) peak. The Laue interference function should give rise to the satellites in both sides of the main peak [15]. On the other hand, Hollanders *et al.* has shown that the high-angle side satellites have significantly smaller intensities than the low-angle ones if the spacing of the diffraction planes is larger at the top and bottom of the crystallite than in the middle part [11]. It is known that the Ti atom has a bigger size than Ni, and the substitutive dissolution of the Ti atoms in Ni increases the Ni lattice by 0.1% per atomic percent of the dissolved Ti [16]. Thus, the observed low-angle satellite peaks of samples 1 and 3 can be explained by the increased spacing at the top and bottom interfaces of the Ni sublayers due to the dissolution of Ti in Ni. The fact of the dissolution of the Ti atoms can be also confirmed by the Ni sublayer thickness dependence of the position of the main diffraction peak of the Ti/Ni MLF (see Fig. 4). The observed peak shift to the low-angle side with decreasing the Ni sublayer thickness is equivalent to an increase of the $d_{Ni(111)}$ spacing for sample Nos. 1 and 3 by 0.59 and

0.89%, respectively. If the same thickness of the interfacial regions with the dissolved Ti atom is presumed for all the Ti/Ni MLF, the average increase in the Ni lattice parameter becomes larger with the thinner nominal thickness of the Ni sublayers.

Figure 5 presents the Ni-sublayer thickness dependence of the $1/\xi$ and $1/\beta$. It is hard to imagine that the grain size in the Ni sublayers is significantly larger than the sublayer thickness. Therefore, it can be supposed that the decrease in t_{Ni} is also accompanied by a decrease in the mean grain size. Thus, it can be presumed that the observed dependence of $1/\xi$ and $1/\beta$ on t_{Ni} reflects a nearly linear decrease in thickness and grain size of the nonreacted Ni sublayers on t_{Ni} in the as-deposited Ti/Ni MLF.

Thus, one can conclude that the as-deposited Ti/Ni MLF with a thick sublayer thickness (sample Nos. 1 and 3) have a certain amount of the dissolved Ti in the interfacial regions, while the Ti/Ni MLF with thinner sublayers form a significantly disordered or amorphous structure (sample No. 5) or a structure with the short-range order or the local environment close to NiTi or Ni_3Ti (sample No. 4). The structure of the reacted zone in the as-deposited Ti/Ni MLF with "thick" sublayers can be considered as highly disordered or amorphous. It should be also concluded that the thickness of the reacted zone in the as-deposited Ti/Ni MLF is hard to be determined quantitatively on the basis of such analyses.

The annealing of the as-deposited Ti/Ni MLF at 580 K for 60 min changes the structure of the films, and hence their low- and high-angle XRD spectra (see Figs. 1–5). According to the results of low-angle XRD study, the layered structure is still preserved in the Ti/Ni MLF after annealing, however, the number of satellites is significantly reduced in the Ti/Ni MLF with "thick"sublayers, while for the Ti/Ni MLF with relatively "thin" sublayers the low-angle XRD patterns are nearly the same as before annealing (see Fig. 1). A prominent shift of the Ni (111) peak for the Ti/Ni MLF with "thick" sublayers by about 0.2 - 0.4° to the high-angle side, and an increase of the peak width is observed in the high-angle XRD patterns. On the other hand, the $2\Theta_{\max}$ for the annealed (3.2 nm Ti / 3.0 nm Ni)$_{60}$ MLF is located at a lower angle than for the corresponding as-deposited one. The shift of the Ni (111) peak to the high-angle side for sample Nos. 1–3 indicates either the restoring of the Ni sublayers to the crystalline structure typical for the thick Ni film due to the annealing or a certain compressive strain in the Ni sublayers. This strain can be induced, for example, by the grain-boundary diffusion of Ti. The high-angle shift of the Ni (111) diffraction peak was also observed by Hollanders *et al.* after an 1-hr annealing and explained by the compressive strain in the Ni sublayers due to an inhomogeneous dissolution of Ti in the contact zone [11].

The broadening of the high-angle XRD peak due to annealing is observed mainly for samples with "thick" sublayers (see Fig. 5a) and can be explained by the diffusion of Ti into the Ni sublayers. Additionally, the fact that the relative increase in $1/\beta$ with t_{Ni} is more noticeable for samples 3–5 than 1 and 2 (see Fig. 5b) allows us to suppose that a reaction of Ni with Ti, caused by annealing, takes place mainly in the Ti/Ni MLF with "thick" sublayers.

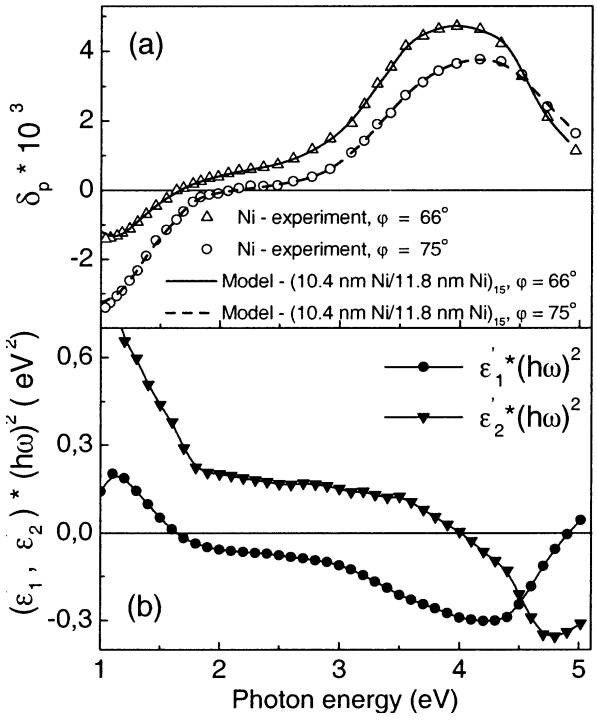

Fig. 6. (a) Experimental EKE spectra for a pure Ni and simulated EKE spectra for a hypothetical (10.4 nm Ni / 11.8 nm Ni)$_{15}$ MLF at $\varphi = 66$ and 75°, and (b) calculated spectra of the off-diagonal components of the DF for the pure Ni film.

The prominent shift of the position of the main diffraction peak for the (3.2 nm Ti / 3.0 nm Ni)$_{60}$ MLF to the low-angle side caused by the annealing can be explained, for example, by the redistribution of the Ti and Ni atoms within the MLF, forming the local order which is close to the cubic TiNi phase ($2\Theta_{\mathrm{NiTi\ (110)}} \approx 42.992°$).

Thus, one can conclude that, in addition to the amorphous layer which is spontaneously formed near the interfaces during the film deposition, the annealing induces the SSR mainly in the Ti/Ni MLF with relatively thick sublayers. At the same time, the mutual dissolution of Ni and Ti in the Ti/Ni MLF with "thin" sublayers is already terminated during the deposition and the annealing leads to only a certain redistribution of the Ti and Ni atoms towards the local environment close to the TiNi type.

3.2 Magneto-optical study

Figure 6 presents the experimental δ_p spectra measured for a pure Ni film at two angles of incidence, and the $\varepsilon_1' \times (\hbar\omega)^2$ and $\varepsilon_2' \times (\hbar\omega)^2$ spectra calculated on the basis of these measurements. ε_1' and ε_2' are the imaginary and real parts, respectively, of the off-diagonal components of the DF. In general, the obtained δ_p, $\varepsilon_1' \times (\hbar\omega)^2$ and $\varepsilon_2' \times (\hbar\omega)^2$

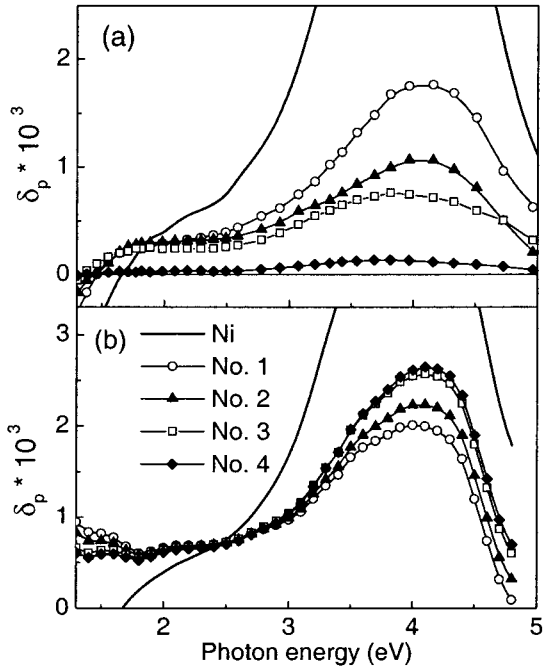

Fig. 7. (a) Experimental and (b) simulated (for the case of sharp interfaces) EKE spectra for the Ti/Ni MLF (samples 1–4) and pure Ni. $\varphi = 66°$.

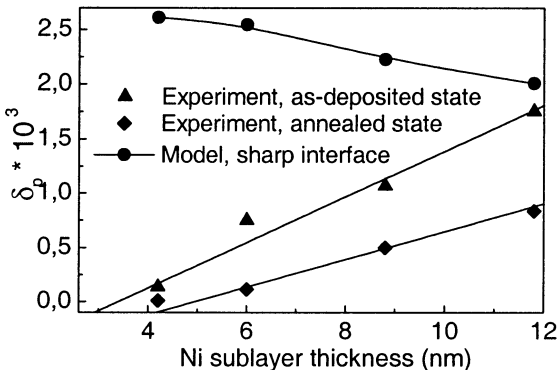

Fig. 8. Ni-sublayer thickness dependence of the simulated (for the case of sharp interfaces) EKE values (circles) of the Ti/Ni MLF and the experimental ones for the as-deposited (triangles) and annealed (diamonds) MLF at $\hbar\omega = 4$ eV and $\varphi = 66°$. Thin solid lines represent linear fits of the experimental dependences.

spectra for the pure Ni film are in a reasonable agreement in the spectrum shape with the corresponding literature data obtained experimentally mainly for the bulk Ni and theoretically for the ideal Ni crystal [17–21]. On the other hand, the intensities of these peaks are nearly twice reduced in comparison with the corresponding peaks for bulk Ni. This difference can be explained by a finer grain structure in the film sample. Indeed, Nikitin *et al.* has studied the EKE spectra of Ni films prepared in the Penning discharge with a simultaneous bombardment by Ar^+, and has shown that the EKE values depend significantly on the deposition conditions and the structure of Ni films [21]. Thus, it is clear that a use of the tabulated MO and optical parameters for bulk Ni and Ti for the simulation of the MO properties of the Ti/Ni MLF might lead to wrong results. The validity of the obtained off-diagonal components of the DF for pure Ni, and of the multireflection approach employed in the simulation were tested by the simulation of the EKE spectrum for the hypothetical (10.4 nm Ni / 11.8 nm Ni)$_{15}$ MLF, *i.e.*, pure Ni. It is seen in Figure 6a that the calculated and experimental EKE spectra coincide perfectly.

Figure 7 presents the results of the experimental study of the EKE for the as-deposited Ti/Ni MLF, together with the modelled EKE spectra calculated for the MLF model with sharp interfaces. It should be mentioned here that the MO response was not experimentally detected for sample Nos. 5 and 6, and for sample No. 7 ($Ti_{0.38}Ni_{0.62}$ alloy film). The result for alloy film can be expected, because in the Ni-Ti alloy system the Curie temperature is known to fall to RT at about 10 at.% of Ti [22]. The experimental EKE spectra conserve all the features of the corresponding spectrum of pure Ni (Fig. 6) but have significantly lower intensities, and also that the magnitude of δ_p for the investigated Ti/Ni MLF decreases with decreasing the nominal Ni sublayer thickness. The Ni-sublayer thickness dependence of the experimental and simulated EKE values at $\hbar\omega = 4$ eV for the Ti/Ni MLF is shown in Figure 8. It seen that they are significantly different. The observed $\delta_p(t_{Ni})$ dependence for the modelled EKE spectra can be explained by an increase of the Ni content in the skin penetration depth (of about 15 nm for 4 eV) with decreasing t_{Ni}. Indeed, owing to the extinction of the electromagnetic wave from the top Ti layer, the MO response from the constituent Ni layers should be larger as the sublayer thicknesses are smaller.

The linear fit of the experimental $\delta_p(t_{Ni})$ dependence for the as-deposited Ti/Ni MLF allows us to determine a threshold value of the nominal Ni-sublayer thickness (t_{Ni}^{th}) for the observation of the EKE to be 3.0 nm. The existence of such a threshold can be explained, for example, by i) the structural transformation in the Ni sublayers below a "critical" thickness, which causes changes in the structure and the magnetic properties of Ni [23,24]; ii) an existence of the so-called "dead" (in the magnetic sense) surface Ni layers neighboring with Ti sublayers [25]; iii) a decrease in the pure Ni sublayer thickness due to the appearance of a nonmagnetic alloy near the interfaces caused by the interdiffusion of the Ti and Ni atoms. The first point can be excluded from the consideration because it presumes an abrupt change in the MO properties near the "critical" thickness.

In general, an agreement in intensity between simulated and experimental EKE spectra for the as-deposited Ti/Ni MLF can be markedly improved by assuming the nonmagnetic alloy-like regions between pure metals in the model structure. Nearly the same correspondence between experimental and modelled EKE spectra can be also obtained by assuming the magnetically "dead" layers of variable thickness at the top and bottom of the Ni sublayers. Figures 9–11 present some examples of these modelled

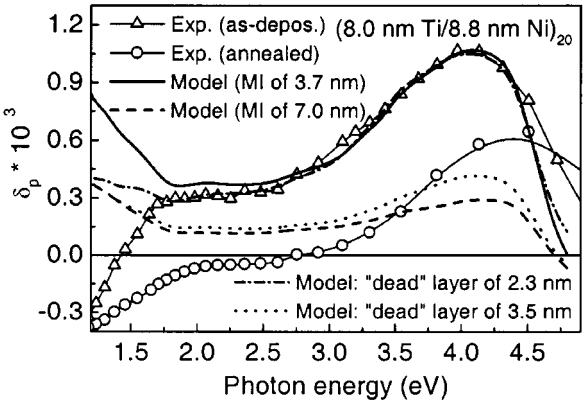

Fig. 9. Experimental EKE spectra for the as-deposited (triangles) and annealed (circles) (8.0 nm Ti / 8.8 nm Ni)$_{20}$ MLF, together with simulated EKE spectra for the models with mixed interface (MI) of 3.7 and 7.0 nm in thickness (thick solid and dashed lines, respectively), and magnetically "dead" layers of 2.3 and 3.5 nm in thickness (thin solid and dotted lines, respectively).

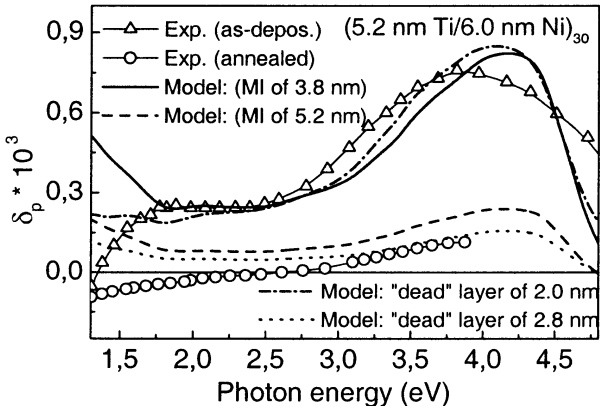

Fig. 10. Experimental EKE spectra for the as-deposited (triangles) and annealed (circles) (5.2 nm Ti / 6.0 nm Ni)$_{30}$ MLF, together with simulated EKE spectra for the models with mixed interface (MI) of 3.8 and 5.2 nm in thickness (thick solid and dashed lines, respectively), and magnetically "dead" layers of 2.0 and 2.8 nm in thickness (thin solid and dotted lines, respectively).

EKE spectra. It is seen that the simulated EKE spectra obtained in the framework of both models are rather similar in shape; some discrepancies between them are observed mainly in the low energy region. This similarity can be explained by the resemblance in the measured optical properties of the pure Ni and $Ti_{0.38}Ni_{0.62}$ films. Both approaches reveal very close results (see Figs. 9–11).

The best correspondence in the spectral shape, and the location and intensity of the UV peak between experimental and simulated EKE spectra was observed for the Ti/Ni MLF with "thick" sublayer thickness (sample No. 1 and, especially, 2 (see Fig. 9)). This fact implies that the actual MO and optical parameters of the Ni and Ti sublayers in such a Ti/Ni MLF are close to those used in the simulation, *i.e.*, the bulk-like values. A decrease in the Ni-sublayer thickness leads to a shift of the experimental UV peak to the low energy side in comparison with the modelled one, and this shift becomes bigger as t_{Ni} is thinner (as seen in Figs. 10 and 11). Such a behavior allows us to suppose that the MO and optical properties of the relatively "thin" sublayers are different from the bulk ones. Among the possible origins for this deviation, an increase in the lattice parameter of Ni can be also considered. In general, the increased lattice parameter should lead to the squeeze of the energy bands towards the Fermi level, reducing the energy interval between initial and final states involved in the peak formation [26]. Indeed, considering the nature of the UV peak in the EKE spectrum of Ni [19,20] the observed shift in the experimental EKE spectra is correlated with the aforementioned shift of the Ni (111) diffraction peak to the low-angle side with decrease in t_{Ni}.

The lack of the MO response for the as-deposited (3.2 nm Ti / 3.0 nm Ni)$_{60}$MLF means that all the Ni atoms are already reacted and a nonmagnetic Ti-Ni alloy is formed or all the ferromagnetic Ni atoms are converted to a magnetically "dead" phase.

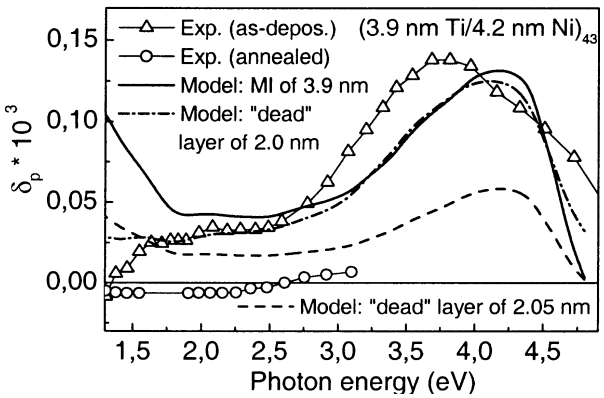

Fig. 11. Experimental EKE spectra for the as-deposited (triangles) and annealed (circles) (3.9 nm Ti / 4.2 nm Ni)$_{43}$ MLF, together with simulated EKE spectra for the models with mixed interface (MI) of 3.9 nm in thickness (thick solid line) and magnetically "dead" layers of 2.0 and 2.05 nm in thickness (thin solid and dashed lines, respectively).

Thus, on the basis of the comparison between experimental and simulated EKE spectra, one can conclude that the actual thickness of the magnetic Ni layers in all the investigated as-deposited Ti/Ni MLF are less than the nominal one. This fact can be explained by the formation of a nonmagnetic Ti-Ni alloy between pure Ti and Ni or by an appearance of the "dead" (in the magnetic sense) Ni layers in the Ni sublayer.

The annealing of the Ti/Ni MLF leads to a noticeable decrease in intensity of the EKE spectra as well as to increase in $t_{\mathrm{Ni}}^{\mathrm{th}}$ up to 4.5 nm (see Figs. 8–11). The MO response for the annealed sample No. 4 was extremely weak: about two orders smaller than that for the pure Ni film (Fig. 11), and we had no technical possibility to measure it at 4 eV. Therefore, the EKE value at $\hbar\omega = 4$ eV for this sample was roughly estimated by extrapolating the experimentally observed $\delta_p(\hbar\omega)$ dependence in the 3–4 eV

energy region for this and other samples. It is also seen in Figure 8 that the relative decrease in the MO response due to the annealing is larger for the Ti/Ni MLF with "thick" sublayers. The simulated (for the case of mixed interfaces) EKE spectra of the annealed (3.9 nm Ti / 4.2 nm Ni)$_{43}$ and (5.2 nm Ti / 6.0 nm Ni)$_{30}$ MLF exceed the experimental ones even if all the Ti sublayers are assumed to be completely reacted (see Figs. 10 and 11). This result also indicates that the MO properties of the very thin (0.3–0.8 nm) nonreacted Ni layers (and hence their electronic structure) differ from the bulk ones.

It is seen that both models (mixed interfaces and "dead"Ni layer) reveal nearly the same result. Some explanations on the nature of the "dead" layer are based on a significant lattice mismatch between neighboring ferromagnetic and nonmagnetic layers [25]. It is hard to imagine that the annealing "kill" additionally many ferromagnetic Ni layers, while the interdiffusion and the formation of a nonmagnetic alloy can. Furthermore, the existence of a Ni "dead" layer of about 10 monolayers itself is not able to be supported by the theory [27]. Therefore, we conclude that the origin for the reduced MO response in the Ti/Ni MLF is the formation of the nonmagnetic TiNi alloy layer near the interfaces during the deposition as well as the heat treatment. The increase in $t_{\mathrm{Ni}}^{\mathrm{th}}$ due to the annealing can be considered as an evidence for the SSR in the Ti/Ni MLF with a consumption of the pure Ni. Unfortunately, we are not in position to provide with the exact structure of the reacted zone by using the results of the MO study.

3.3 Optical study

The experimental spectra of optical conductivity (OC, σ) and real part (ε_1) of the diagonal components of the DF for the as-deposited Ti/Ni MLF, and pure Ni and Ti films are shown in Figure 12. The optical properties of Ni have been widely investigated experimentally [28–30], and the observed features were explained in terms of band structures [19,20,31]. The OC spectrum for the bulk Ni is characterized by an intense absorption peak in the UV region and a smaller peak at 1.4 eV. The OC spectrum for the Ni film obtained in the present work also exhibits a prominent absorption peak near 4.4 eV but its intensity is lower than for the bulk Ni, and the 1.4 eV peak is not seen at all. As in case of the MO properties, we think that the decrease in magnitude of both peaks is the consequence of the fine grain structure of the film. The optical properties of pure Ti are also well known [32–34]. The OC spectrum for the single-crystalline hcp Ti exhibits a group of intense peaks in an energy range of 1–3 eV [34]. As aforementioned, the prepared Ti film has a nearly amorphous structure. Therefore, instead of an intense peak at 2 eV (which is typical for the OC spectrum of the single-crystalline Ti), a broad and tiny shoulder on the Drude-like background is observed for the OC spectrum of the Ti films. The ε_1 spectra for the Ni and Ti films show no bright feature except a gradual increase in absolute value with decreasing photon energy (being always negative).

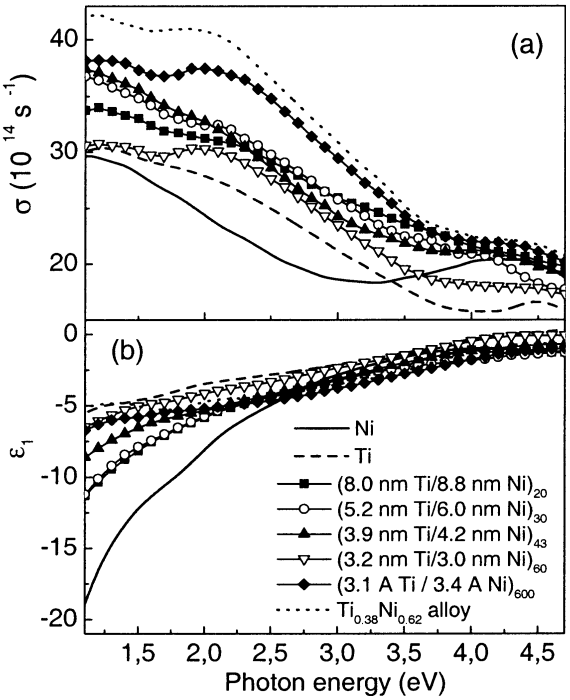

Fig. 12. Experimental (a) optical conductivity and (b) ε_1 spectra for the as-deposited Ti/Ni MLF, and pure Ni and Ti films.

The optical properties of the Ti/Ni MLF with "thick" sublayers (sample Nos. 2 and 3) do not exhibit any new features in the σ and ε_1 spectra in comparison with corresponding spectra of the Ti and Ni films. Because the 4.4 eV OC absorption peak of the pure Ni film is located at the same energy as the local OC minimum of the Ti film, the Ni peak is weakly manifested in the experimental OC spectra for the Ti/Ni MLF. The ε_1 spectra for sample Nos. 2 and 3 also lie between the frames marked by the corresponding spectra for the Ni and Ti films. A decrease in the sublayer thickness of the Ti/Ni MLF leads to a gradual change of both σ and ε_1 experimental spectra mainly in the visible and near IR regions: the thinner nominal thickness of the sublayers, the smaller absolute value of ε_1 and the more prominent OC absorption peak near 2.2 eV, revealing all the features of the σ and ε_1 spectra for the $Ti_{0.38}Ni_{0.62}$ alloy film (sample No. 7). Such a behavior of the optical properties clearly shows the growth of regions with the alloyed components in the as-deposited Ti/Ni MLF with decreasing the sublayer thickness, and confirms the conclusions made on the basis of the XRD and MO studies. This conclusion is also supported by a comparison with the literature data for the optical properties of the equiatomic TiNi alloy.

According to the phase diagram for the bulk Ni-Ti alloys, $Ti_{0.38}Ni_{0.62}$ alloy consists of the mixture of the TiNi and $TiNi_3$ phases. It was shown that the OC spectra of both possible phases of the equiatomic Ni-Ti alloy (*i.e.*, with $B2$ and $B19'$ types of structure) are characterized by an intense peak at ~ 2.26 eV and an abrupt decrease of σ in the IR region [35,36]. Therefore, we suppose that the peak near 2.2 eV in the OC spectra of the $Ti_{0.38}Ni_{0.62}$ alloy

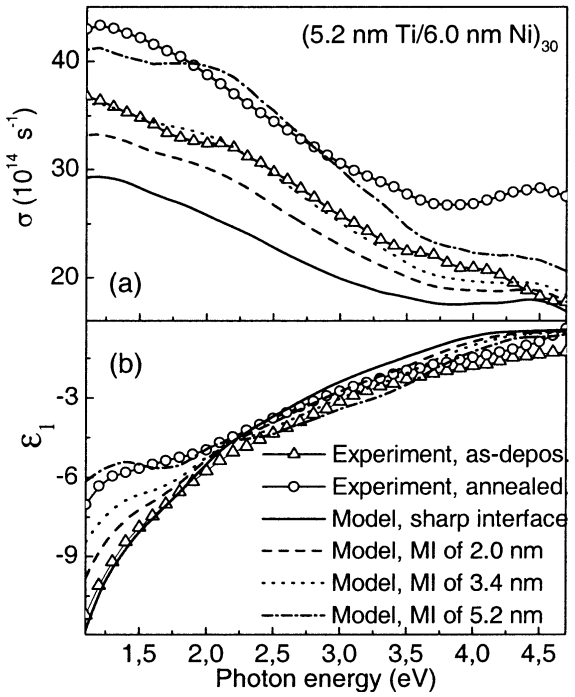

Fig. 13. Experimental and simulated (a) optical conductivity and (b) ε_1 spectra for the as-deposited (triangles) and annealed (circles) (5.2 nm Ti / 6.0 nm Ni)$_{30}$ MLF. Solid, dashed, dotted and dashed-dotted lines represent the corresponding simulated spectra for the models of MLF with sharp and mixed interfaces (MI) of 2.0, 3.4 and 5.2 nm in thickness, respectively.

film (sample No. 7) originates from the regions with the local environment close to the TiNi phase, and that the growth of the OC values with decreasing photon energy is due to the $TiNi_3$ phase.

Because all the investigated Ti/Ni MLF exhibit nearly the same regularities for the changes in the optical properties caused by the annealing, we will discuss only one of them, *i.e.*, (5.2 nm Ti / 6.0 nm Ni)$_{30}$ MLF. Figure 13 illustrates our attempts to interpret the optical properties of the as-deposited and annealed (5.2 nm Ti / 6.0 nm Ni)$_{30}$ MLF in the framework of the electromagnetic model.

It is seen that a reasonable agreement between simulated and experimental optical properties for the as-deposited (5.2 nm Ti / 6.0 nm Ni)$_{30}$ MLF can be obtained either for the σ spectra using the model with alloyed interfaces of 3.4 nm in thickness or for the ε_1 spectra using the model with alloyed interfaces of 2.0 nm in thickness. It is thought that this uncertainty is possibly caused by surface oxidation of the samples. Nevertheless, in general, we can conclude that, according to the results of the optical study, all the as-deposited Ti/Ni MLF have the alloyed interfacial regions between pure components, and these results are in an agreement with the mentioned conclusions based on the XRD and MO studies.

The annealing of the Ti/Ni MLF leads to prominent changes in the σ and ε_1 spectra of all the investigated MLF. The common features of these changes are: i) a decrease in the absolute value of ε_1 at $\hbar\omega < 2.0$ eV; ii) a reduced intensity or even the disappearance of the peak at 2.2 eV in the σ spectra; iii) and also the appearance of a feature (an interband absorption peak) in the UV region. While the ε_1 spectra of the Ti/Ni MLF are changed towards that of the $Ti_{0.38}Ni_{0.62}$ alloy (see Fig. 12), which reflects the formation of an amorphous alloy, the others ones can not be explained by such a process. It should be reminded here that the agreement between experimental and modelled EKE spectra for the annealed Ti/Ni MLF was also significantly worse than that for the as-deposited ones. Therefore, it can be also supposed that the sublayers in the annealed Ti/Ni MLF have different optical (and MO) properties from those used in the simulations, *i.e.*, the bulk-like ones. These deviations may be caused by, for example, strains or changes in the lattice parameter in the very thin pure Ni or Ti sublayers due to the SSR process.

Here, we must note that, besides exhibiting their own small features, in general, the OC and ε_1 spectra of the Ni and Ti films as well as the $Ti_{0.38}Ni_{0.62}$ alloy film are rather similar (see Fig. 12), showing a low "optical contrast" between themselves. This fact can be considered as unlucky circumstance for the Ti/Ni MLF system, which embarrasses the use of optical spectroscopy for the quantitative interface analyses.

4 Conclusions

1. The study of the SSR in the Ti/Ni MLF has been performed by using the experimental and computer simulated MO and optical spectroscopies as well as XRD.

2. The optical and MO properties for pure Ni and Ti films were determined experimentally and compared with the corresponding properties of bulk Ni and Ti. It was shown that they are noticeably different and that a use of the tabulated MO and optical parameters related to bulk Ni and Ti might lead to wrong results for the simulation of the MO properties of the Ti/Ni MLF.

3. It was shown that alloyed-like regions in an amorphous structure is spontaneously formed near the interfaces between pure elements during the MLF fabrication. The thickness of this region was estimated as 2–3.8 nm on the basis of the results of the MO and partially optical studies. On the other hand, a conclusion that these alloyed regions are amorphous was made on the basis of the XRD and partly optical investigations.

4. It was shown that the SSR in the Ti/Ni MLF caused by an annealing at 580 K for 60 min increases the thickness of these interfacial amorphous regions mainly in the Ti/Ni MLF with "thick" sublayers. This result means that, in the Ti/Ni MLF with thinner sublayers, the SSR occurs spontaneously during the film deposition.

5. The spectral and sublayer-thickness dependences of the MO and optical properties of the Ti/Ni MLF were investigated experimentally and explained on the basis of the electromagnetic theory.

6. It was also suggested that the very thin nonreacted Ni sublayers have different MO properties (and hence electron energy structure) from the bulk.

7. Because the constituent layers, *i.e.*, Ni, Ti and Ti-Ni alloy of the Ti/Ni MLF have rather similar optical properties, the use of optical spectroscopy for studying the SSR looks inappropriate for the case of the Ti/Ni MLF, which shows a less sensitivity than the other employed techniques.

Authors thank to C.S. Kim for the XRD measurements. This work was supported by a Korea Research Foundation Grant (KRF-99-D00048).

References

1. F. Mezei, Proc. Soc. Photo-Opt. Instrum. Eng. **83**, 10 (1988).
2. C.F. Majkrzak, J.L. Wood, in *SPIE Proceedings on Neutron Optical Devices and Applications*, 1992, p. 1738.
3. M.S. Kumar, P. Böni, S. Texier, Physica B **248**, 53 (1998).
4. B.M. Clemens, Phys. Rev. B **33**, 7615 (1986).
5. B.E. White, Jr., M.E. Patt, E.J. Cotts, Phys. Rev. B **42,** 11017 (1990).
6. E.J. Cotts, W.J. Meng, W.L. Johnson, Phys. Rev. Lett. **57**, 2295 (1986).
7. B. Blanpain, L.H. Allen, J.-M. Legresy, J.W. Mayer, Phys. Rev. B **39**, 13067 (1989).
8. M. Vedpathak, S. Basu, S. Gokhale, S.K. Kulkarni, Thin Solid Films **335**, 13 (1998).
9. C. Brouder, G. Krill, P. Guilmin, G. Marchal, E. Daryge, A. Fontaine, G. Tourillon, Phys. Rev. B **37**, 2433 (1988).
10. S. Kraegermann, K. Chrzumnicka, F. Stobiecki, H. Rohrmann, K. Roll, J. Magn. Magn. Mater. **140-144**, 593 (1995).
11. M.A. Hollanders, B.J. Thijsse, E.J. Mittemeijer, Phys. Rev. B **42**, 5481 (1990).
12. Y. P. Lee, R. Gontarz, Y. V. Kudryavtsev, Phys. Rev. B, **63,** 144402 (2001).
13. R.M.A. Azzam, N.M. Bashara, *Ellipsometry and Polarized Light* (North-Holland, Amsterdam, 1977).
14. *Powder Diffraction Data*, edited by Joint Committee on Powder Diffraction Standards (Swarthmore, PA, 1960).
15. B.E. Warren, *X-Ray Diffraction* (Addison-Wesley, Reading, MA, 1969).
16. W.B. Pearson, *Handbook of Lattice Spacing and Structures of Metals and Alloys* (Pergamon, Oxford, 1958).
17. G.S. Krinchik, V.A. Artm'ev, Zh. Eksp. Teor. Fiz. **53**, 1901 (1967) [Sov. Phys. JETP, **26**, 1080 (1968)].
18. G.S. Krinchik, V.S. Gushchin, Zh. Eksp. Teor. Fiz. **56**, 1833 (1969).
19. Y.A. Uspenski, S.V. Khalilov, Zh. Eksp. Teor. Fiz. **95,** 1022 (1989) [Sov. Phys. JETP, **68**, 588 (1989)].
20. P.M. Oppeneer, T. Maurer, J. Sticht, J. Kübler, Phys. Rev. B **45**, 10924 (1992).
21. L.V. Nikitin, E.V. Likhushina, S.V. Svechnikov, G.V. Smirnitskaya, J. Magn. Magn. Mater. **148**, 102 (1995).
22. R.M. Bozorth, *Ferromagnetism* (IEEE Press, New York, 1993), p. 325.
23. J. Dubowik, F. Stobiecki, H. Rohrmann, K. Roell, J. Magn. Magn. Mater. **122**, 201 (1996).
24. Y.V. Kudryavtsev, A.Y. Kucherenko, J. Dubowik, F. Stobiecki, Y.P. Lee, J. Vac. Sci. Technol. A **16**, 389 (1998).
25. Y. Kwon, T.H. Rho, S.C. Hong, Y.P. Lee, J. Korean Phys. Soc. **35**, S47 (1999).
26. J.Y. Rhee, K.W. Kim, Y.V. Kudryavtsev, Y.P. Lee, J. Korean Phys. Soc. **35**, S578 (1999).
27. A.M.N. Niklasson, B. Johansson, H. L. Skriver, Phys. Rev B **59,** 6371 (1999).
28. H. Ehrenreich, H.P. Philipp, D.J. Olechna, Phys. Rev. **131**, 2469 (1963).
29. M. Shiga, G.P. Pells, J. Phys. C **2**, 1847 (1969).
30. M.M. Kirillova, Zh. Eksp. Teor. Fiz. **61**, 336 (1971).
31. C.S. Wang, J. Callaway, Phys. Rev. B **9**, 4897 (1974).
32. I.D. Mash, G.P. Motulevich, Zh. Eksp. Teor. Fiz. **63**, 985 (1972).
33. D.W. Lynch, C.G. Olson, J.H. Weaver, Phys. Rev. B **11**, 3617 (1975).
34. V.N. Antonov, M.M. Kirillova, E.E. Krasovskii, L.D. Kurmaeva, N.V. Minulina, Fiz. Met. Metalloved., Iss. 6, 83 (1990).
35. I.I. Sasovskaya, S.A. Shabalovskaya, A.I. Lotkov, Zh. Eksp. Teor. Fiz. **77**, 2341 (1979) [Sov. Phys. JETP **50**, 1128 (1979)].
36. J.Y. Rhee, B.N. Harmon, D.W. Lynch, Phys. Rev. B **59**, 1878 (1999).